Inorganic Chemistry

Article

pubs.acs.org/IC

Multidimensional (0D to 3D) Alkaline-Earth Metal Diphosphonates: Synthesis, Structural Diversity, and Luminescence Properties

Duraisamy Senthil Raja,[†,+] Pin-Chun Lin,[‡,+] Wei-Ren Liu,*[,‡] Jun-Xiang Zhan,[†] Xin-Yi Fu,[†] and Chia-Her Lin*[,†]

[†]Department of Chemistry and [‡]Department of Chemical Engineering, Chung-Yuan Christian University, Chungli 320, Taiwan

Supporting Information

ABSTRACT: A series of new alkaline-earth metal diphosphonate frameworks were successfully synthesized under solvothermal reaction condition (160 °C, 3 d) using 1-hydroxyethylidene-1,1-diphosphonic acid ($CH_3C(OH)(H_2PO_3)_2$, $hedpH_4$) as a diphosphonate building block and Mg(II), Ca(II), Sr(II), or Ba(II) ions as alkaline-earth metal ion centers in water, dimethylformamide, and/or EtOH media. These diphosphonate frameworks, $(H_2NMe_2)_4[Mg(hedpH_2)_3]\cdot 3H_2O$ (**1**), $(H_2NMe_2)_2[Ca(hedpH_2)_2]$ (**2**), $(H_2NMe_2)_2[Sr_3(hedpH_2)_4(H_2O)_2]$ (**3**), and $[Ba_3(hedpH_2)_3]\cdot H_2O$ (**4**) exhibited interesting structural topologies (zero-, one-, two-, and three-dimensional (0D, 1D, 2D, and 3D, respectively)), which are mainly depending on the metal ions and the solvents used in the synthesis. The single-crystal analysis of these newly synthesized compounds revealed that **1** was a 0D molecule, **2** has 1D chains, **3** was a 3D molecule, and **4** has 2D layers. All compounds were further characterized using thermogravimetric analysis, solid-state ^{31}P NMR, powder X-ray diffraction analysis, UV−vis spectra, and infrared spectroscopy. In addition, Eu(III)- and Tb(III)-doped compounds of **1**−**4**, namely, $(H_2NMe_2)_4[Ln_xMg_{1-x}(hedpH_2)_2(hedpH_{2-x})]\cdot 3H_2O$ (**1Ln**), $(H_2NMe_2)_2[Ln_xCa_{1-x}(hedpH_2)(hedpH_{2-x})]$ (**2Ln**), $(H_2NMe_2)_2[Ln_xSr_{3-x}(hedpH_2)_3(hedpH_{2-x})(H_2O)_2]$ (**3Ln**), and $[Ln_xBa_{3-x}(hedpH_2)_2(hedpH_{2-x})]\cdot H_2O$ (**4Ln**) (where Ln = Eu, Tb), were synthesized, and their photoluminescence properties were studied. The quantum yield of **1Eu**−**4Eu** was measured with reference to commercial red phosphor, $Y_2O_2S:Eu^{3+}$ (YE), and the quantum yield of terbium-doped compounds **1Tb**−**4Tb** was measured with reference to commercial green-emitting phosphor $CeMgAl_{10}O_{17}:Tb^{3+}$. Interestingly, the compound **2Eu** showed very high quantum yield of 92.2%, which is better than that of the reference commercial red phosphor, YE (90.8%).

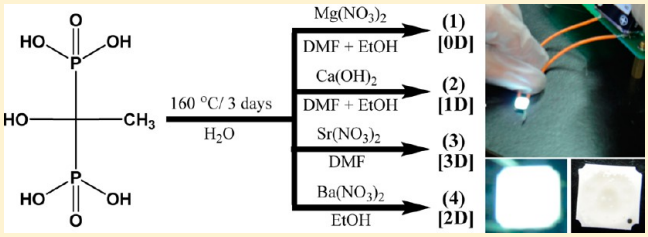

INTRODUCTION

In the last few decades, the inorganic−organic hybrid materials have attracted interest among chemists because of their diverse structural features and their numerous applications in various fields.[1−12] These frameworks are usually constructed by metal ions or metal clusters connected through organic linkers such as polycarboxylates,[9] phosphonates,[1,6,10] sulfonates,[11] and amines.[12] In this regard, metal phosphonates showed a greater variety of structural motifs than that of metal carboxylates in a same combination of metal ion and linker case, because the degree of deprotonation of the phosphonate ligands are mostly controlled by the reaction pH, which is very much influenced their coordination properties, and the phosphonate ligands have an additional oxygen over carboxylate ligands, which makes more coordination possible.

On the other hand, the attention on metal phosphonate materials has increased in recent times due to the interesting structures of metal phosphonates[13−20] and their promising applications in catalytic systems,[21−23] anticorrosion,[24] making clean energy,[25] adsorption and separation,[26−29] sensor,[30] luminescent materials,[30−34] proton conduction,[34−36] magnetic materials,[37−40] biological systems,[41] semiconductors,[42,43] and so on. The interesting point here is that these applications are mostly influenced by the structure of the phosphonates. In this context, metal diphosphonates are getting limelight in recent years; for example, diphosphonates are applied as calcification inhibitors[44] and for bone cancer theraphy.[45] On considering the diphosphonic acids, 1-hydroxyethylidene-1,1-diphosphonic acid ($CH_3C(OH)(H_2PO_3)_2$, $hedpH_4$) is a well-known diphosphonic acid, and the presence of the hydroxyl group in $hedpH_4$ makes an additional coordination possible in its metal complexes. A number of reports dealing with the crystal structural chemistry of metal diphosphonates having $hedpH_4$ as ligand were found in the literature.[46−60] The structures of these reported metal diphosphonates are mostly made up of metal-oxide polyhedra, layers, or chains. So far, only few alkaline-earth metal-hedp complexes have been reported,[46−50] and there is no systematic investigation on the reactions of alkaline-earth metal ions with $hedpH_4$ ligand without adding any template molecules or bases.

Our aim is to examine the coordination behavior of $hedpH_4$ on constructing the alkaline-earth metal diphosphonate frameworks and study their properties. Hence, we present herein the optimized synthetic conditions, characterizations (including

Received: December 15, 2014
Published: April 14, 2015

DOI: 10.1021/ic5029993
Inorg. Chem. 2015, 54, 4268−4278

single-crystal structural analysis), and properties of a series of alkaline-earth metal diphosphonate frameworks, namely, $(H_2NMe_2)_4[Mg(hedpH_2)_3]\cdot 3H_2O$ (**1**), $(H_2NMe_2)_2[Ca(hedpH_2)_2]$ (**2**), $(H_2NMe_2)_2[Sr_3(hedpH_2)_4(H_2O)_2]$ (**3**), and $[Ba_3(hedpH_2)_3]\cdot H_2O$ (**4**). These frameworks display interesting structural features (zero-, one-, two-, and three-dimensional (0D, 1D, 2D and 3D, respectively)) that depend on the metal ions and the solvents used in the synthesis (Scheme 1). Further, the photoluminescence properties of europium- and terbium-doped compounds of **1**−**4**, namely, $(H_2NMe_2)_4[Ln_xMg_{1-x}(hedpH_2)_2(hedpH_{2-x})]\cdot 3H_2O$ (**1Ln**), $(H_2NMe_2)_2[Ln_xCa_{1-x}(hedpH_2)(hedpH_{2-x})]$ (**2Ln**), $(H_2NMe_2)_2[Ln_xSr_{3-x}(hedpH_2)_3(hedpH_{2-x})(H_2O)_2]$ (**3Ln**), $[Ln_xBa_{3-x}(hedpH_2)_2(hedpH_{2-x})]\cdot H_2O$ (**4Ln**) (where Ln = Eu, Tb), were evaluated.

Scheme 1. Schematic Representation of Structural Diversity in Alkaline-Earth Metal Diphosphonates Reported in This Paper

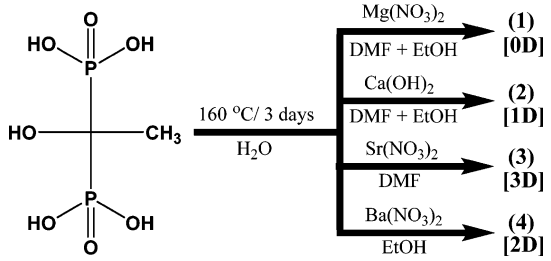

EXPERIMENTAL SECTION

Materials and General Methods. All the chemicals used in this work were purchased commercially with maximum purity and used as such. The 23 mL Teflon bombs were used for all the solvothermal reactions. All the reaction mixtures were heated at the rate of 60 °C h^{-1} under pressure to reach 160 °C; after that, the temperature was maintained at 160 °C for 3 d and then slowly (at the rate of 6 °C h^{-1}) cooled to room temperature. The phase purity of all the compounds was examined with the aid of powder X-ray diffraction (PXRD) measurements using PANalytical X'pert PRO X-ray diffractometer. PE-2400 CHN Elemental analyzer was used for elemental analyses. Total reflection X-ray fluorescence (TXRF) spectra were measured on a Bruker S2 PICOFOX equipped with Mo excitation with a high-efficiency module. JASCO FT/IR-460 spectrometer was used to measure the IR spectrum of our compounds in the form of solid KBr matrix, which are measured in the range of 4000−400 cm^{-1}. Thermogravimetric analysis (TGA) was done on the powder sample of the compounds under N_2 atmosphere with 10 °C min^{-1} heating rate using DuPont TA Q50 analyzer instrument. The solid-state ^{31}P NMR spectra were recorded using a Bruker DSX 400 spectrometer instrument. $BaSO_4$ plate was used as internal standard for measuring UV−vis spectra, which were done using Varian Cary 100 UV−vis spectrophotometer instrument. Photoluminescence spectra of the lanthanide-doped compounds were measured using a HITACHI F-4500 FL spectrophotometer instrument, and the excitation and emission slit widths were maintained as 2.5 mm for all the measurements.

Synthesis of $(H_2NMe_2)_4[Mg(hedpH_2)_3]\cdot 3H_2O$ (1). The compound **1** was achieved using the reaction mixture containing $hedpH_4$ (60%, 1 mL, 3 mmol), $Mg(NO_3)_2\cdot 6H_2O$ (0.256 g, 1 mmol), dimethylformamide (DMF, 7.0 mL), EtOH (2.0 mL), and H_2O (1.0 mL), having pH of 1.64. Yield: 0.672 g (76.8%, based on Mg). Anal. Calcd for $C_{14}H_{56}MgN_4O_{24}P_6$: C, 19.22; H, 6.45; N, 6.40. Found: C, 19.15; H, 6.56; N, 6.38%. IR (KBr, cm^{-1}): 3340(br), 3224(s), 2790(m), 2442(m), 2303(m), 1620(m), 1470(w), 1414(w), 1249(w), 1147(s), 1089(s), 915(s), 859(w), 813(w), 653(w), 539(m), 490(m).

Synthesis of $(H_2NMe_2)_2[Ca(hedpH_2)_2]$ (2). Compound **2** was synthesized from a reaction mixture containing $hedpH_4$ (60%, 0.5 mL, 1.5 mmol), $Ca(OH)_2$ (0.0371 g, 0.5 mmol), DMF (7.0 mL), EtOH (2.0 mL), and H_2O (1.0 mL), having pH of 3.01. Yield: 0.253 g (93.7%, based on Ca). Anal. Calcd for $C_8H_{28}CaN_2O_{14}P_4$: C, 17.78; H, 5.22; N, 5.18. Found: C, 17.60; H, 5.28; N, 5.19%. IR (KBr, cm^{-1}): 3425(br, s), 3124(m), 2802(m), 2300(w), 1749(w), 1714(w), 1680(w), 1635(w), 1519(w), 1478(w), 1370(w), 1222(w), 1126(m), 1078(m), 1038(m), 919(m), 828(w), 795(w), 681(w), 650(w), 563(w), 453(w).

Synthesis of $(H_2NMe_2)_2[Sr_3(hedpH_2)_4(H_2O)_2]$ (3). The colorless crystals of **3** were achieved from a reaction mixture of $hedpH_4$ (60%, 0.5 mL, 1.5 mmol), $Sr(NO_3)_2$ (0.106 g, 0.5 mmol), DMF (5.0 mL), and H_2O (1.0 mL), having pH of 2.47. Yield: 0.513 g (84.9%, based on Sr). Anal. Calcd for $C_{12}H_{44}N_2O_{30}P_8Sr_3$: C, 11.94; H, 3.67; N, 2.32. Found: C, 11.82; H, 3.61; N, 2.24%. IR (KBr, cm^{-1}): 3423(m), 3120(m),

Table 1. Selected Crystallographic Analysis Data for 1−4

	1	2	3	4
chemical formula	$C_{14}H_{56}MgN_4O_{24}P_6$	$C_8H_{28}CaN_2O_{14}P_4$	$C_{12}H_{44}Sr_3N_2O_{30}P_8$	$C_6H_{20}Ba_3O_{22}P_6$
formula weight	874.75	540.29	1207.12	1042.03
space group	$R\bar{3}c$	$P2_1/n$	$C2/c$	$P\bar{1}$
a, Å	16.5827(6)	5.7106(2)	22.5561(8)	10.7703(8)
b, Å	16.5827(6)	15.3214(7)	17.4368(6)	10.8543(7)
c, Å	52.106(2)	12.3862(6)	10.1995(4)	13.1677(15)
α, deg	90	90	90	113.854(4)
β, deg	90	102.893(2)	109.4020(10)	93.428(4)
γ, deg	90	90	90	114.852(3)
volume, $Å^3$	12408.8(8)	1056.40(8)	3783.7(2)	1227.55(18)
Z	12	4	8	2
D_{cacl}, gcm^{-3}	1.427	1.699	2.096	2.819
μ, mm^{-1}	0.357	0.669	4.657	5.247
T, °C	295(2)	295(2)	295(2)	295(2)
reflections collected	23792	9443	14066	22156
independent reflections	3465	2603	4726	6036
R(int)	0.0481	0.0617	0.0435	0.0516
λ, Å	0.710 73	0.710 73	0.710 73	0.710 73
$R1$	0.0566	0.0322	0.0294	0.0226
$wR2$	0.1788	0.0832	0.0850	0.0509
CCDC	1037690	1037691	1037692	1037693

DOI: 10.1021/ic5029993
Inorg. Chem. 2015, 54, 4268−4278

1656(m), 1460(m), 1172(s), 1073(s), 1019(m), 937(m), 901(s), 882(s), 818(w), 637(w), 546(m), 508(m), 448(m).

Synthesis of $[Ba_3(hedpH_2)_3]\cdot H_2O$ (4). A reaction mixture of $hedpH_4$ (60%, 0.5 mL, 1.5 mmol), $Ba(NO_3)_2$ (0.131 g, 0.5 mmol), EtOH (5.0 mL), and H_2O (1.0 mL) having pH value of 2.95 was used to get colorless crystals of compound **4**. Yield: 0.453 g (86.9%, based on Ba). Anal. Calcd for $C_6H_{20}Ba_3O_{22}P_6$: C, 6.92; H, 1.93. Found: C, 7.01; H, 1.94%. IR (KBr, cm^{-1}): 3433(br, s), 1638(m), 1459(w), 1163(s), 901(s), 798(w), 644(w), 554(m), 468(s).

Synthesis of Lanthanide-Doped Compounds of 1−4, $(H_2NMe_2)_4[Ln_xMg_{1-x}(hedpH_2)_2(hedpH_{2-x})]\cdot 3H_2O$ (1Ln), $(H_2NMe_2)_2[Ln_xCa_{1-x}(hedpH_2)(hedpH_{2-x})]$ (2Ln), $(H_2NMe_2)_2[Ln_xSr_{3-x}(hedpH_2)_3(hedpH_{2-x})(H_2O)_2]$ (3Ln), $[Ln_xBa_{3-x}(hedpH_2)_2(hedpH_{2-x})]\cdot H_2O$ (4Ln) (where Ln = Eu, Tb). Ln(III) chlorides (20 mol %) along with the similar combinations of reagents and molar ratios as that used in the syntheses of compounds **1**−**4** were used.

Single-Crystal Structure Analysis. The single-crystal diffraction data for the compounds were collected on Bruker AXS KAPPA APEX II diffractometer equipped with Mo Kα radiation having λ = 0.71073 Å and graphite monochromator. Systematic absences and statistics of intensity distribution were used to determine the space group for all the compounds. All the structures were solved using metal atom being located first, followed by the O, N, and C atoms found on successive difference Fourier maps. The hydrogen atoms were included in ideal positions to ride with their parent atoms. *SHELXTL* programs in *APEX2*[61] were used for all the calculations. The selected crystallographic analysis data are tabulated in Table 1 (compounds **1**−**4**) and Table 2 (compounds **3Eu** and **3Tb**). Selected M(II)−O bond lengths are listed in Table S1 (Supporting Information). The corresponding H-bonding data are listed in Table S2 (Supporting Information).

Table 2. Crystallographic Data for 3Eu and 3Tb

	3Eu	3Tb
formula	$C_6H_{20.08}NO_{15}P_4Sr_{1.29}Eu_{0.21}$	$C_6H_{20.07}NO_{15}P_4Sr_{1.29}Tb_{0.21}$
fw	614.80	616.85
space group	*C*2/*c*	*C*2/*c*
a, Å	22.3119(7)	22.2858(7)
b, Å	17.3774(5)	17.3710(5)
c, Å	10.1854(3)	10.1701(3)
α, deg	90	90
β, deg	110.2950(10)	110.425(2)
γ, deg	90	90
volume, $Å^3$	3703.95(19)	3689.59(19)
Z	8	8
D_{cacl}, g cm^{-3}	2.205	2.221
μ, mm^{-1}	4.847	4.971
collection *T* (K)	295(2)	295(2)
reflctions collected	21118	21237
independent reflections	4622	4533
R(int)	0.0320	0.0352
λ, Å	0.710 73	0.710 73
R_1	0.0482	0.0534
wR_2	0.1235	0.1500
CCDC	1037694	1037695

RESULTS AND DISCUSSION

Synthesis and Characterization. All four compounds were synthesized under same solvothermal reaction condition (160 °C, 3 d). In all the cases, a particular $hedpH_4$−metal salt molar ratio (2:1) was optimized to produce better yield. Note that the compounds **1**−**3** are anionic complexes, whereas the compound **4** is a neutral complex, which may due to absence of DMF solvent in the reaction. The phase purities of the synthesized compounds (**1**−**4**) were confirmed by PXRD patterns, which show essential peaks matching with calculated ones (Figures S1−S4, Supporting Information). The IR spectra of the compounds showed peak shifts and intensity differences in the phosphonate moiety spectral region (880−1250 cm^{-1}, Figure S9, Supporting Information), which were verified later by the crystal-structural analysis. The solid-state UV−vis spectra of the compounds exhibited intraligand charge transfer transition peaks for all compounds at room temperature (Figure S10, Supporting Information). Further, the PXRD patterns of lanthanide-doped compounds of **1**−**4Ln** were measured and compared with their original ones (Figures S5−S8, Supporting Information). The PXRD peaks of lanthanide-doped compounds almost match with their undoped compounds, but, very few low-intensity peaks were also found, which may be due to presence of low amount of unidentified phase. Total reflection X-ray fluorescence (TXRF) analyses were used to determine the Eu/Tb content in lanthanide-doped compounds. The TXRF analyses showed that the molar ratios of M/Eu are 94.5:5.5, 92.5:7.5, 92.5:7.5, and 88.0:12.0 for **1**−**4Eu**, respectively, and the molar ratios of M/Tb are 94.3:4.7, 92.7:7.3, 92.3:7.7, and 86.5:13.5 for **1**−**4Tb**, respectively (where M represents the corresponding alkaline earth metal). Hence, the results of TXRF analyses of **1**−**4Ln** confirmed the presence of Eu/Tb in **1**−**4Ln**. Further confirmation of doping of Eu/Tb in the compounds was drawn from the single-crystal structural analysis of compounds **3Eu** and **3Tb**, which are discussed in the coming structural description part.

Structural Description of $(H_2NMe_2)_4[Mg(hedpH_2)_3]\cdot 3H_2O$ (1). The compound **1** crystallizes in a rhombohedral space group $R\bar{3}c$, which is very rare among the reported metal diphosphonates. The structure of **1** has 0D framework. Each asymmetric unit of **1** contains one-third Mg(II) ion, a $(hedpH_2)^{2-}$ unit, a lattice H_2O molecule, along with four-thirds lattice dimethylammonium (DMA) cation $[(H_2NMe_2)^+]$ (which is formed from the amide reduction of DMF solvent during course of the reaction[62]). The Mg atom is coordinated to six O atoms of three hedp ligand units, which forms a distorted octahedral coordination geometry (Figure 1a). Each hedp ligand is coordinated to only one Mg atom through O1 and O4 phosphonate oxygen atoms (Figure 1b). The Mg−O bond distances range from 2.046(2) to 2.110(2) Å (Table S1, Supporting Information), which agrees well with the Mg(II)-phosphonate reports.[63] As shown in Figure 1c, each MgO_6 octahedra is corner-shared with six phosphonate tetrahedra. The whole unit is further interconnected to each other through various hydrogen bonds involving oxygen atom of lattice water molecule, nitrogen atom of lattice DMA cation, and the oxygen atoms of $(hedpH_2)^{2-}$ ligand unit to form a stable 0D molecular architecture. (Figure 1d, Table S2, Supporting Information). It is interesting to note the various types of H-bonding in **1**: (i) the intermolecular H-bonding between the hydrogen atoms of the phosphonate group of the one ligand unit and three oxygen atoms of the other ligand unit (O2−H1···O3, O6−H2···O5, and O7−H3···O1)—which reduces the degree of flexibility of the hedp ligand to some extent; (ii) hydrogen bonds between the lattice water hydrogen atoms and the oxygen atoms (O6 and O7) of the phosphonate group—these hydrogen bonds stabilize the H_2O position in the crystal lattice; (iii) the H-bonding between the H atoms with N atom in dimethylammonium cations and O atoms of the ligand unit (N1−H4···O5, N1−H5···O4, and N1−H5···O6).

DOI: 10.1021/ic5029993
Inorg. Chem. 2015, 54, 4268−4278

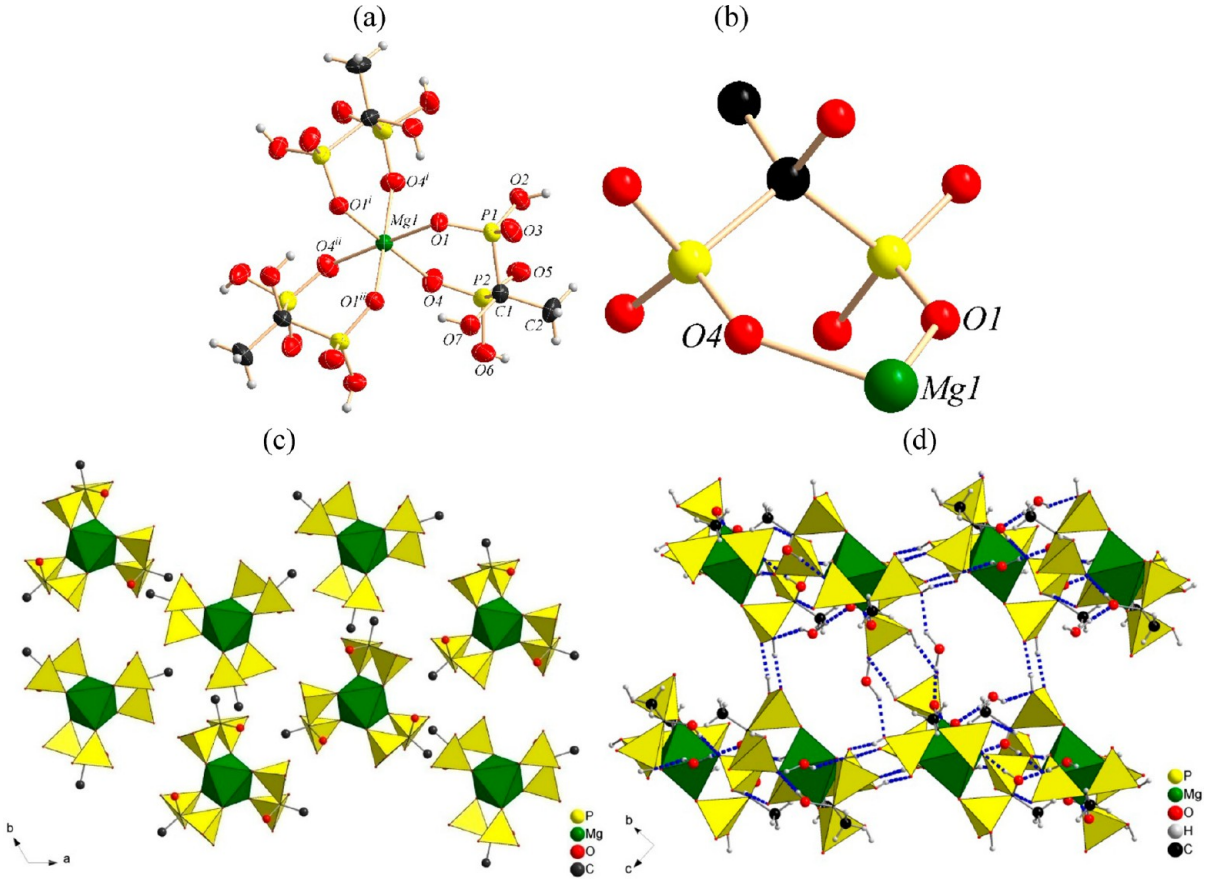

Figure 1. (a) The coordination environment of the Mg atom of **1** (symmetry codes: (i) $-x+y, -x, z$; (ii) $-y, x-y, z$). (b) The coordination mode of the ligand in **1**. (c) The whole structural view of **1** along the *c*-axis. (d) The view of different modes of H-bonding interaction in **1** along *a*-axis.

Structural Description of $(H_2NMe_2)_2[Ca(hedpH_2)_2]$ (2). Compound **2** crystallizes in a monoclinic space group $P2_1/n$. The asymmetric unit of **2** contains half of crystallographically distinct calcium site, one $hedpH_2$ site, and one lattice DMA cation. The Ca atom is coordinated to six O atoms of four $hedpH_2$ ligand units, which forms a distorted octahedral coordination geometry (Figure 2a). The Ca−O bond lengths are from 2.3230(13) to 2.3606(2) Å (Table S1, Supporting Information), which is similar to that of reported calicium diphosphonates.[49] The $(hedpH_2)^{2-}$ unit is bonded with two Ca atoms through three of its O1, O2, and O6 phosphonate oxygen atoms (Figure 2b). As shown in bottom of Figure 2c, each CaO_6 octahedra is corner-shared with six phosphonate tetrahedra and connected to each other through two corner-shared phosphonate tetrahedra, which forms infinite 1D chain structure running along *a*-axis. The 1D chain unit in **2** is further interconnected through various hydrogen bonds involving nitrogen atoms of lattice DMA cation, and the oxygen atoms of $(hedpH_2)^{2-}$ ligand unit (O3−H1···O5, O4−H2···O1, O4−H2···O2, O7−H3···O6, N1−H4···O2, and N1−H5···O5; Figure 2d and Supporting Information, Table S2).

Structural Description of $(H_2NMe_2)_2[Sr_3(hedpH_2)_4(H_2O)_2]$ (3). The crystal structure of **3** possesses extended 3D framework structure having monoclinic space group of $C2/c$. Each asymmetric unit of **3** has crystallographically distinct one and half Sr sites, two $hedpH_2$ sites, a coordinated H_2O moiety, and a lattice DMA cation. The Sr1 atom is coordinately bonded to eight phosphonate oxygen atoms belonging to four ligand units (Figure 3a). On the other hand, the Sr2 is seven-coordinated in which it is coordinated to six phosphonate O atoms of four $(hedpH_2)^{2-}$ units and one O atom of a water molecule (Figure 3a). Two kinds of $(hedpH_2)^{2-}$ units are in **3**: one is bonded with two Sr2 atoms through three of its phosphonate O atoms (O7, O8 and O13), and the another is bonded with two Sr1 and two Sr2 atoms through four of its O1, O2, O4, and O5 phosphonate O atoms. (Figure 3b). The Sr−O bond length range, from 2.478(2) to 2.7448(19) Å (Table S1, Supporting Information), is similar to that of reported Sr-phosphonates.[63] The $Sr1O_8$ polyhedron is face-shared with two $Sr2O_7$ polyhedron in opposite direction through O1, O4, and O5 of phosphonate O atoms (Figure S11, Supporting Information). The whole unit is further interconnected with neighboring similar units in all three directions through $(hedpH_2)^{2-}$ ligand units that form the 3D framework of **3** (Figure S12a, Supporting Information). There is an existence of porosity in **3** along the *c*-axis (Figure S12a, Supporting Information). Two lattice DMA cations are found in the porous channels. A number of H-bondings are found in the framework of **3**, which is presented in Figure S12b and Table S2 (Supporting Information). After the removal of DMA cations and water molecules in the pores of **3** by PLATON,[64] the 1D channel along the *c*-axis has a cross-sectional area of 4.28 × 10.42 $Å^2$, and the calculated solvent-accessible volume is 1311.4 $Å^3$, which is ∼34.7% of total unit cell volume, which is shown in Figure 3c.

Structural Description of $(H_2NMe_2)_2[Ln_xSr_{3-x}(hedpH_2)_3(hedpH_{2-x})(H_2O)_2]$ (3Ln). As determined by the single-crystal structural analysis, the compounds **3Eu** and **3Tb** are found to be isostructural with compound **3**. For comparison, the selected structural refinement data for **3Eu** and **3Tb** are

DOI: 10.1021/ic5029993
Inorg. Chem. 2015, 54, 4268−4278

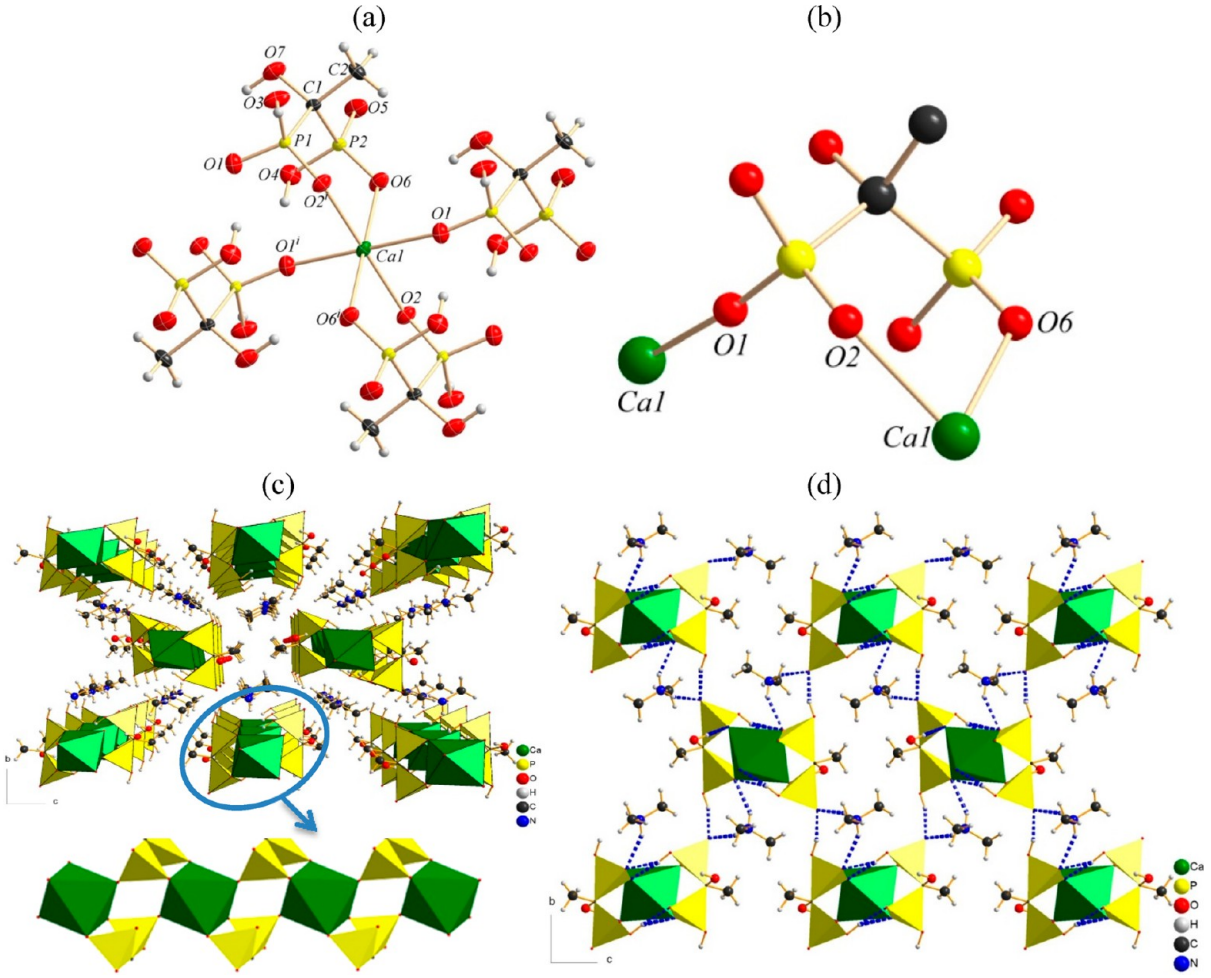

Figure 2. (a) The coordination environment of the Ca atom of **2** (symmetry code: (i) $-x+1, -y, -z$). (b) The coordination mode of the ligand in **2**. (c) The whole structural view of **2** along the *a*-axis. (d) The view of different modes of H-bonding interaction in **2** along *a*-axis.

tabulated in Table 2. In the structure of **3Eu** and **3Tb**, the divalent Sr(1) atomic sites were partially occupied by Eu(III) and Tb(III), respectively; hence, we assumed the H atoms on hydroxyl group were partly deprotonated for charge balance as shown in the formula. During the single-crystal structure analysis, we found that 42% of Sr(1) sites were found to be occupied by Eu(III) or Tb(III).

Structural Description of $[Ba_3(hedpH_2)_3]\cdot H_2O$ (4). The asymmetric unit of **4** contains three crystallographically distinct barium atoms, three $(hedpH_2)^{2-}$ units, and a lattice H_2O molecule. The Ba1 atom is coordinated to 10 oxygen atoms belonging to four different $(hedpH_2)^{2-}$ ligands of which seven are phosphonate oxygen atoms, and the remaining three are O19, O20, and O21 atoms of hydroxyl group (Figure 4a); whereas, the Ba2 atom is coordinated to nine phosphonate O atoms from six $(hedpH_2)^{2-}$ ligands (Figure 4a). In the case of nine coordinated Ba3 atoms, nine phosphonate oxygen atoms belonging to four different $(hedpH_2)^{2-}$ ligands are participated in coordination with Ba3 atom (Figure 4a). There are three kinds of $(hedpH_2)^{2-}$ units that are found in **4**; one is bonded with two Ba1 and Ba2 atoms along with one Ba3 atom using five of its O4, O6, O13, O14, and O15 phosphonate oxygen atoms and hydroxyl oxygen atom (O20); the second one is bonded with two Ba2 atoms and each one of Ba1 and Ba3 atoms through four of its phosphonate O1, O2, O3, and O17 atoms and hydroxyl O20 atom; the third one is bonded with two Ba2 and Ba3 and a Ba1 atom through four of its phosphonate O atoms (O7, O10, O11, and O12) and hydroxyl oxygen atom (O22, Figure 4b). The $Ba1O_{10}$ polyhedron is face-shared with $Ba2O_9$ and $Ba3O_9$ polyhedron through three of its phosphonate O atoms (O3, O4, and O13; and O7, O10, and O15, respectively), which form the trinuclear Ba_3O_{22} cluster basic unit of **4** (Figure S13a, Supporting Information). This trinuclear Ba_3O_{22} unit is directly connected with four neighboring similar units (Figure S13b, Supporting Information), and in the same way, each unit is connected with other neighboring units along *a*- and *b*-axes, along with ligand units connections form the 2D sheet framework of **4** (Figure 4c). The 2D layers are connected with each other through various H-bondings, which is depicted in Figure 4d and Table S2 (Supporting Information).

Evaluation of Structural Diversity. The structural analysis of these four alkaline-earth metal diphosphonates derived from 1-hydroxyethylidene-1,1-diphosphonic acid as a diphosphonate building block and four different alkaline-earth metals led to some fascinating structural features. The diphosphonate building unit leads to various structural features from 0D molecular architecture to 3D frameworks depending upon the alkaline-earth metal ion types (Scheme 1). It is interesting to note that the ligand acted as binegative $(hedpH_2^{2-})$ in all the cases, which may be due to the similar pH (1.64−3.01) of all the reactions. Though all the reactions reported in this article were performed in almost similar conditions, the coordination mode of the ligand was

DOI: 10.1021/ic5029993
Inorg. Chem. 2015, 54, 4268−4278

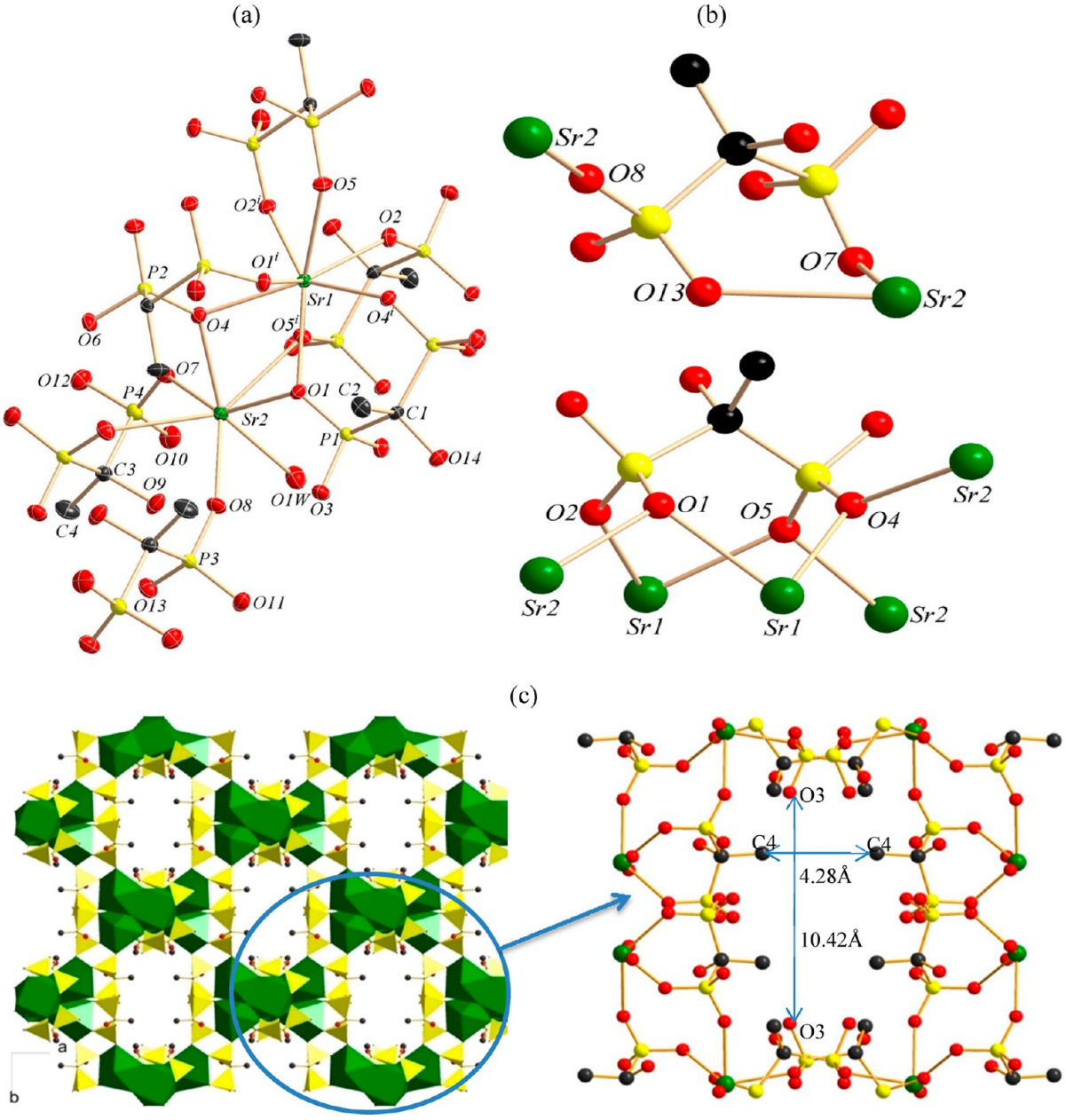

Figure 3. (a) The coordination environment of the Sr atoms in **3** (symmetry code: (i) $-1/2+x, -1/2-y, -3/2+z$). (b) The coordination mode of the ligands in **3**. (c) The 1D porous channels in the framework of **3** along *c*-axis after the removal of DMA cations and water molecules.

different toward each metal ions, which leads to the observed diversity in the alkaline-earth metal diphosphonate structures. The simple coordination modes of ligand, "μ_1" and "μ_2" in **1** and **2**, leads to the formation of 0D or 1D molecular architecture in our alkaline-earth metal diphosphonates, whereas complicated and multiple coordination modes of ligand, "μ_4" and "μ_5" in **3** and **4** lead to the formation of 2D or 3D molecular frameworks. Further, except **4**, the complexes **1**−**3** are anionic in nature, which may be due the DMF solvent; the DMF used as solvent in the reactions was reduced to DMA during reaction and acted as DMA cation to neutralize the charge of the complexes **1**−**3**.

Solid-State NMR Measurements. The compounds **1**−**3** are further characterized using ^{31}P NMR spectra, which are shown in Figure 5. The solid-state ^{31}P NMR spectrum of compound **1** showed a peak at 19.51 ppm that is due to the presence of two P (P1 and P2) atoms (which are NMR equivalent) in its asymmetric unit. Since the two phosphonate P atoms in **2** are having slightly different chemical environment, there are two peaks found at 19.35 and 17.74 ppm for P1 and P2 atoms, respectively, in the ^{31}P NMR spectrum of **2**. The ^{31}P NMR spectrum of compound **3** showed four peaks at 11.10, 15.56, 17.00, and 23.48 ppm, which conform the presence of four chemically distinct P atoms in **3**. Hence, the ^{31}P NMR spectral studies further support the single-crystal structure of compounds **1**−**3**.

Thermal Stability. To examine the architectural and thermal stability of the newly synthesized compounds (**1**−**4**), TGA performed on the compounds of **1**−**4** and their corresponding TGA curves are given in Figure 6. The TGA curve of **1** showed that the first weight loss (7.1%) at 110 °C, which may corresponded to the loss of three lattice H_2O (ca. 6.2%). After that, compound **1** starts to degrade in unresolved steps indicating

DOI: 10.1021/ic5029993
Inorg. Chem. 2015, 54, 4268−4278

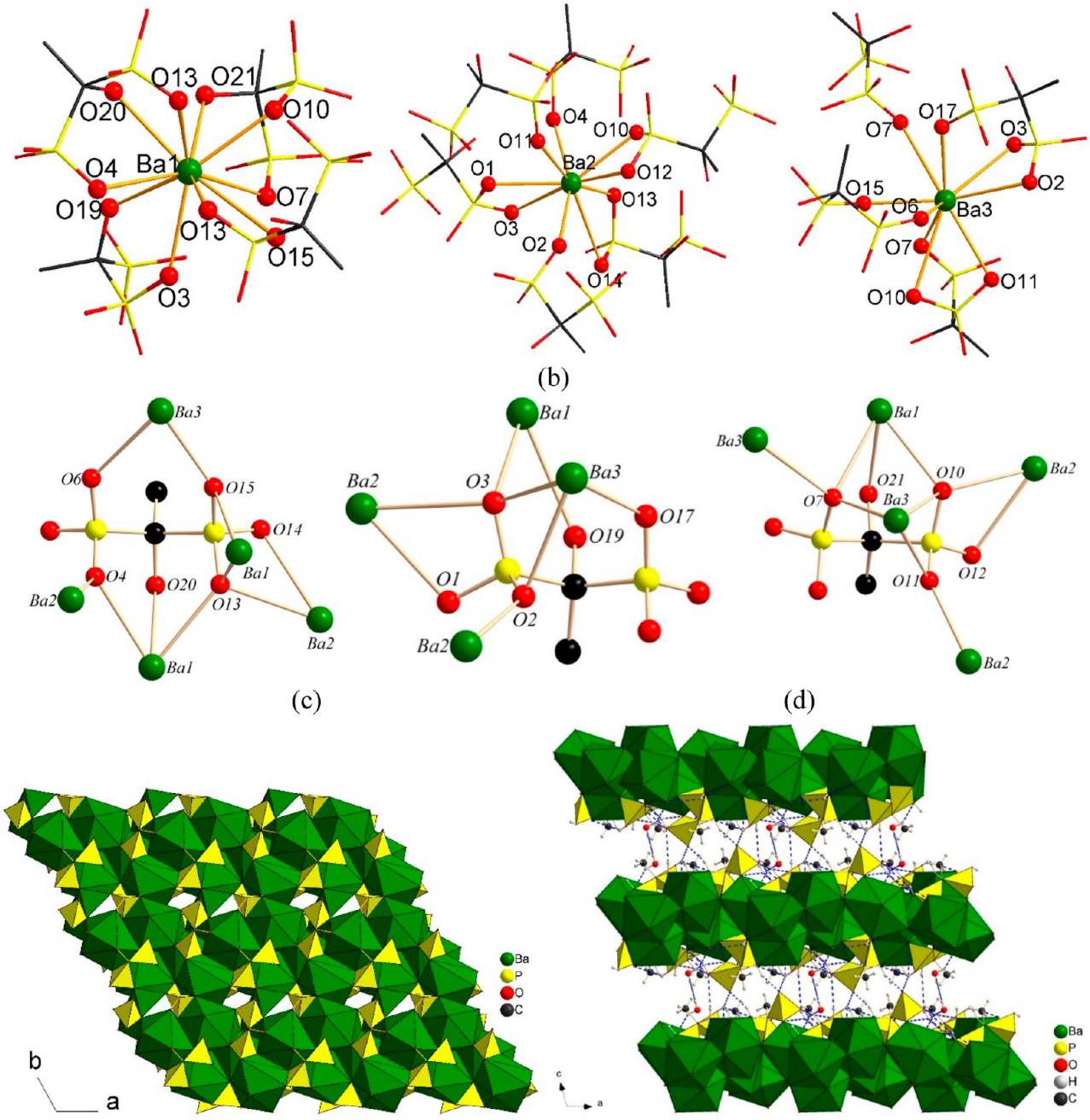

Figure 4. (a) The coordination environment of the Ba atoms in **4**. (b) The coordination mode of the ligands in **4**. (c) The structural view of **4** along the *c*-axis. (d) The view of different modes of H-bonding interaction in **4**.

the loss of DMA cations first followed by the decomposition of remaining organic ligand. The weight loss of 40.2% is observed at the temperature range of 110−600 °C for **1**. Further heating of **1** to 800 °C resulted $Mg_2P_2O_7$ as determined by comparison of its PXRD pattern with the PXRD pattern of JCPDF No. 751055 in JCPDS database (Figure S14, Supporting Information).[65] Since compound **2** has no lattice solvent molecules, there is no weight loss observed in its TGA curves up to 200 °C; hence, the **2** is stable on heating to 200 °C. The first weight loss of 17.2% at 300 °C indicated the loss of two DMA cations in **2**. The further heating of **2** above 300 to 800 °C resulted the decomposition of **2** and forms the amorphous powder (weight loss from 300 to 800 °C is 22.7%). In the TGA curve of **3**, the weight loss of 3% (ca. 2.98%) observed up to 200 °C is most probably due to the loss of two weakly bonded H_2O. The second stage weight loss of 8.3% at 200−280 °C indicated the loss of two DMA cations (ca. 7.6%). The weight loss of 16.3% observed from 280 to 600 °C for **3** is indicated the decomposition of organic ligands in **3**. The heating of **3** to 800 °C yielded the $Sr_2P_2O_7$ as determined by comparison of its PXRD pattern with the PXRD pattern of JCPDF No. 721419 in JCPDS database (Figure S15, Supporting Information).[65] On the other hand, the compound **4** is stable on heating to ∼350 °C, and only ∼1.6% weight loss has been observed, which corresponds to the loss of one lattice H_2O (ca. 1.7%). Further heating of **4** to 800 °C resulted the decomposition of organic ligand in two steps and formed the unidentified amorphous powder.

DOI: 10.1021/ic5029993
Inorg. Chem. 2015, 54, 4268−4278

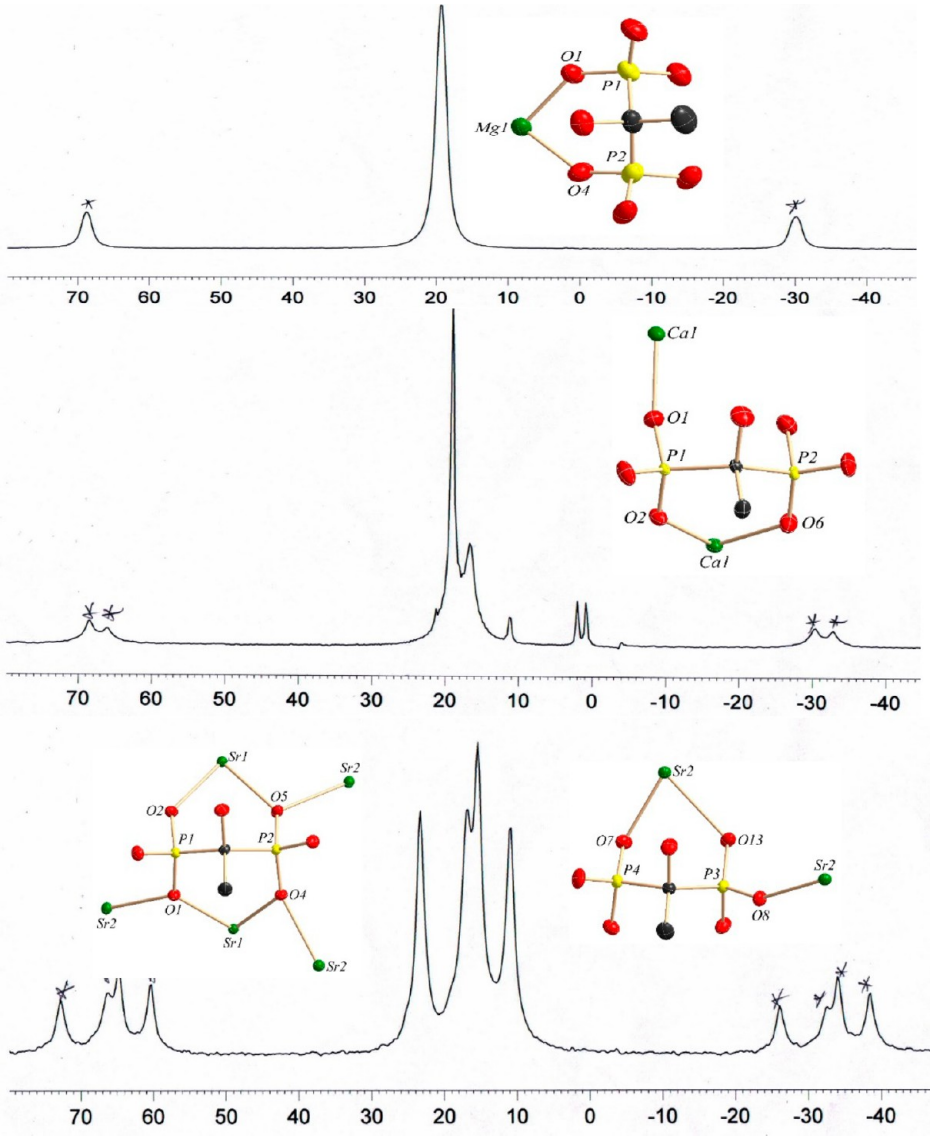

Figure 5. ^{31}P NMR for **1** (upper), **2** (middle), and **3** (lower) (* indicates spinning sideband).

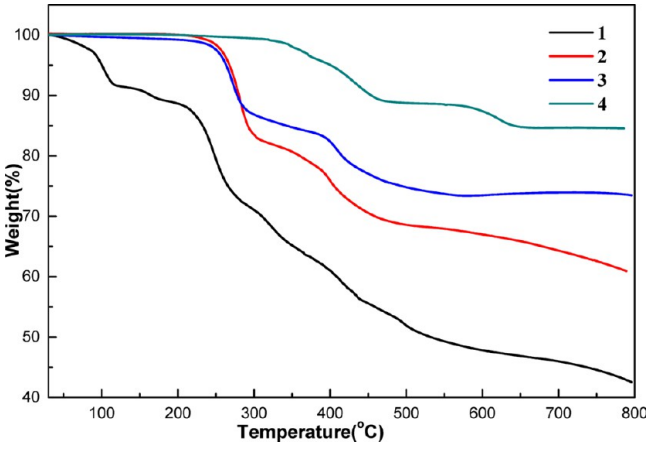

Figure 6. TGA curves for the compounds **1**–**4**.

Photoluminescence Characteristics of Europium/Terbium-Doped Compounds. The compounds **1**–**4** do not show any fluorescence properties, and, hence, the compounds **1**–**4** were doped with lanthanides, namely, europium and terbium (**1Ln**–**4Ln**), and their photoluminescence properties were evaluated. The excitation and emission wavelengths of compounds **1Ln**–**4Ln** are given in Table 3.

The room-temperature photoluminescence spectra of **1Eu**–**4Eu** showed common distinct features (see Figure S16, Supporting Information). The spectra of **1Eu**–**4Eu** recorded at the excitation wavelength of 394 nm showed characteristic bands of Eu(III) at 594, 614, 653, and 701–702 nm, which may be due

Table 3. Excitation and Emission Wavelengths in the Photoluminescence Spectra of Compounds 1Ln–4Ln

compound	excitation (λ_{max})	emission (λ_{max})
1Eu	394 nm	594, 614, 653, 701 nm
2Eu	394 nm	594, 614, 653, 702 nm
3Eu	394 nm	594, 614, 653, 702 nm
4Eu	394 nm	594, 614, 653, 702 nm
1Tb	378 nm	491, 546, 585, 622 nm
2Tb	378 nm	491, 546, 585, 621 nm
3Tb	370 nm	491, 546, 585, 621 nm
4Tb	370 nm	491, 546, 585, 622 nm

DOI: 10.1021/ic5029993
Inorg. Chem. 2015, 54, 4268–4278

to $^5D_0 \rightarrow {}^7F_1$, $^5D_0 \rightarrow {}^7F_2$, $^5D_0 \rightarrow {}^7F_3$, and $^5D_0 \rightarrow {}^7F_4$ transitions, respectively.[66] The strong intensity observed for $^5D_0 \rightarrow {}^7F_2$ peak together with a very weak $^5D_0 \rightarrow {}^7F_0$ peak, witnessed as a shoulder peak at the $^5D_0 \rightarrow {}^7F_1$ transition, indicates the presence of lower-symmetry site.[67] As we saw in the Eu(III)-doped compounds, the photoluminescence spectra of all the Tb(III)-doped compounds (**1Tb**−**4Tb**) also have similar emission bands to each other (Figure S17, Supporting Information). The emission spectra of terbium-doped compounds exhibited characteristic bands of terbium(III) compounds at 491, 546, 585, and 621−622 nm, which correspond to $^5D_4 \rightarrow {}^7F_6$, $^5D_4 \rightarrow {}^7F_5$, $^5D_4 \rightarrow {}^7F_4$, and $^5D_4 \rightarrow {}^7F_3$ transitions, respectively,[66] and the shape of the spectrum agrees with that of [Tb(HPMIDA)-$(H_2O)_2$]·H_2O emission spectrum.[68] Since the compounds **1**, **3**, and **4** have lattice/coordinated water molecules, the emission spectra of the dehydrated **1Ln**, **3Ln**, and **4Ln** were measured and compared with the hydrated compounds. The results indicated that the luminescence spectra of dehydrated **1Ln**, **3Ln**, and **4Ln** have similar emission peaks with little change in their intensity compared to those of the corresponding hydrated compounds (Figure S18, Supporting Information). Further, the quantum yield (QY) of **1Eu**−**4Eu** was measured with reference to commercial red phosphor—$Y_2O_2S:Eu^{3+}$ (YE), and the QY of terbium doped compounds **1Tb**−**4Tb** was measured with reference to commercial green-emitting phosphor $CeMgAl_{10}O_{17}:Tb^{3+}$ (CAT); the corresponding values are tabulated in Tables 4 and 5, respectively.

Table 4. QY Measurements for the Compounds 1Eu−4Eu

	YE[a]	1Eu	2Eu	3Eu	4Eu
absorbance (%)	60.9	16.7	17.4	15.8	28.1
QY (%)	90.8	69.7	92.2	76.2	6.5

[a]YE = $Y_2O_2S:Eu^{3+}$

Table 5. QY Measurements for the Compounds 1Tb−4Tb

	CAT[a]	1Tb	2Tb	3Tb	4Tb
absorbance (%)	22.5	18.7	21.4	25.2	26.1
QY (%)	94.7	59.4	58.7	67.8	2.8

[a]CAT = $CeMgAlO_{19}:Tb^{3+}$

From the QY values (Table 4), it is interesting to note that **2Eu** showed very high quantum efficiency among the four compounds studied, and the QY of **2Eu** (92.2%) is slightly higher than that of the reference commercial red phosphor YE (having QY of 90.8%). In the case of QY of Tb-doped compounds (Table 5), except **4Tb**, the other three compounds showed good QY values (~60 to 70%) which are less than that of the reference commercial green phosphor CAT (94.7%). Overall, the QY values of all the compounds (except **4Eu** and **4Tb**) are much better than some of our reported lanthanide-doped compounds.[63]

To test the commercial significance of our lanthanide-doped compounds, we made two 380 nm light-emitting diodes (LEDs) using **1Eu** and **1Tb** (as representative), respectively. Figure 7a,c shows the LED packages by solely using these red- and green-emitting compounds. Figure 7b,d demonstrates the CIE coordinates and photo images of **1Eu** and **1Tb**, respectively, in UV box under excitation at 365 nm. The CIE coordinates of **1Eu** and **1Tb** are (0.6580, 0.3417) and (0.3564, 0.5578), respectively. These results demonstrate that our compounds could be potential green-emitting and red-emitting phosphors for near-ultraviolet commercial LED applications.

CONCLUSION

In this work we have studied the role of alkaline-earth metal ions to control the structure of their diphosphonate frameworks using a flexible diphosphonic acid ligand. We have synthesized four new alkaline-earth metal diphosphonates containing 1-hydroxyethylidene-1,1-diphosphonic acid, which were prepared by similar solvothermal synthetic conditions. The structural differences between these alkaline-earth metal diphosphonates indicate the key role of solvents and the alkaline-earth metal ions in determining the structure of these diphosphonate frameworks. Moreover, the photoluminescence properties of lanthanide (Eu and Tb)-doped compounds (**1**−**4Ln**) have also been explored. The QY measurements revealed that the Eu-doped compound **2Eu** showed very high QY of 92.2%, which is better than that of the reference commercial red phosphor YE (90.8%). Further, the LEDs made by using **1Eu** and **1Tb** showed that these compounds could be potential phosphors for commercial LED applications.

ASSOCIATED CONTENT

Supporting Information

Illustrated PXRD patterns, FT-IR, UV−vis absorption, and photoluminescence spectra, additional structural diagrams for **3** and **4**, tables concerning selected bond lengths and hydrogen bonding length data for **1**−**4**, and crystallographic information files. This material is available free of charge via the Internet at http://pubs.acs.org.

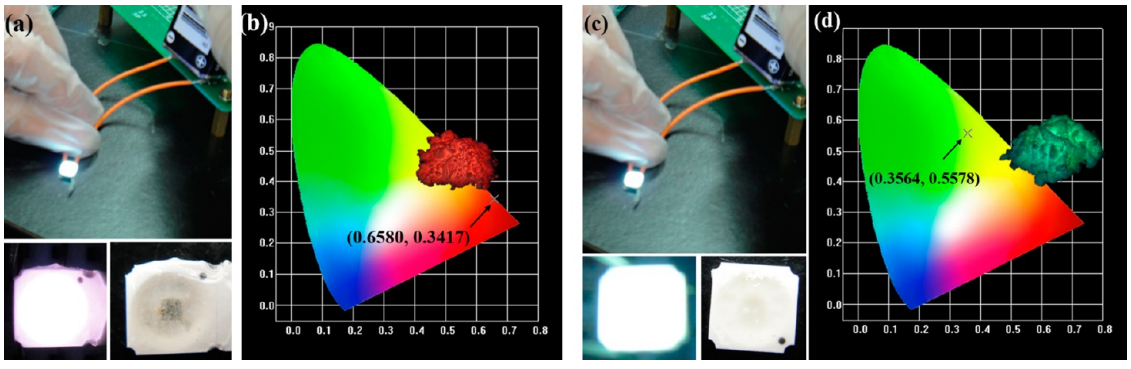

Figure 7. LED packages by using 380 nm near-UV chip in conjunction with and **1Eu** (a) and **1Tb** (c). (b, d) The corresponding CIE coordinates and photo images of **1Eu** and **1Tb** excited by 365 nm in UV box.

DOI: 10.1021/ic5029993
Inorg. Chem. 2015, 54, 4268−4278

AUTHOR INFORMATION

Corresponding Authors

*E-mail: wrliu1203@gmail.com. (W.R.L.)

*E-mail: chiaher@cycu.edu.tw. Phone: +886-3-2653315. Fax: 886-3-2653399. (C.H.L.)

Author Contributions

+These authors contributed equally.

Notes

The authors declare no competing financial interest.

ACKNOWLEDGMENTS

Financial assistance received from the Ministry of Science and Technology, Taiwan (NSC101-2113-M-033-007-MY3 and MOST103-2632-M-033-001-MY3), is gratefully acknowledged.

REFERENCES

(1) Gagnon, K. J.; Perry, H. P.; Clearfield, A. *Chem. Rev.* **2012**, *112*, 1034−1054.

(2) Cheetham, A. K.; Rao, C. N. R.; Feller, R. K. *Chem. Commun.* **2006**, 4780−4795.

(3) Maughan, A. E.; Kurzman, J. A.; Neilson, J. R. *Inorg. Chem.* **2015**, *54*, 370−378.

(4) Choi, Y. C.; Mandal, T. N.; Yang, W. S.; Lee, Y. H.; Im, S. H.; Noh, J. H.; Seok, S. I. *Angew. Chem., Int. Ed.* **2014**, *53*, 1329−1333.

(5) Zhang, Z.; Chen, Y.; Xu, X.; Zhang, J.; Xiang, G.; He, W.; Wang, X. *Angew. Chem., Int. Ed.* **2014**, *53*, 429−433.

(6) Leidinger, P.; Simonato, S.; Feldmann, C. *Chem. Commun.* **2012**, *48*, 7046−7048.

(7) Eguchi, R.; Uchida, S.; Mizuno, N. *Angew. Chem., Int. Ed.* **2012**, *51*, 1635−1639.

(8) Sanchez, C.; Belleville, P.; Popall, M.; Nicole, L. *Chem. Soc. Rev.* **2011**, *40*, 696−753.

(9) Li, M.; Li, D.; O'Keeffe, M.; Yaghi, O. M. *Chem. Rev.* **2014**, *114*, 1343−1370.

(10) Kinnibrugh, T. L.; Bakhmutov, V. I.; Clearfield, A. *Cryst. Growth Des.* **2014**, *14*, 4976−4984.

(11) Thuéry, P. *Inorg. Chem.* **2013**, *52*, 435−447.

(12) Yang, S.; Zhu, X.; Zhou, S.; Wang, S.; Feng, Z.; Wei, Y.; Miao, H.; Guo, L.; Wang, F.; Zhang, G.; Gua, X.; Mu, X. *Dalton Trans.* **2014**, *43*, 2521−2533.

(13) Feyand, M.; Seidler, C. F.; Deiter, C.; Rothkirch, A.; Lieb, A.; Wark, M.; Stock, N. *Dalton Trans.* **2013**, *42*, 8761−8770.

(14) Białek, M. J.; Janczak, J.; Zoń, J. *CrystEngComm* **2013**, *15*, 390−399.

(15) Gagnon, K. J.; Prosvirin, A. V.; Dunbar, K. R.; Teat, S. J.; Clearfield, A. *Dalton Trans.* **2012**, *41*, 3995−4006.

(16) Perry, H. P.; Gagnon, K. J.; Law, J.; Teat, S.; Clearfield, A. *Dalton Trans.* **2012**, *41*, 3985−3994.

(17) Schmidt, C.; Stock, N. *Inorg. Chem.* **2012**, *51*, 3108−3118.

(18) Taddei, M.; Costantino, F.; Vivani, R.; Sangregorio, C.; Sorace, L.; Castelli, L. *Cryst. Growth Des.* **2012**, *12*, 2327−2335.

(19) Tang, S.-F.; Li, L.-J.; Lv, X.-X.; Wang, C.; Zhao, X.-B. *CrystEngComm* **2014**, *16*, 7043−7052.

(20) Matczak-Jon, E.; Videnova-Adrabinska, V. *Coord. Chem. Rev.* **2005**, *249*, 2458−2488.

(21) Zhu, Y.-P.; Ren, T.-Z.; Yuan, Z.-Y. *RSC Adv.* **2015**, *5*, 7628−7636.

(22) He, S.; Liu, X.; Zhao, H.; Zhu, Y.; Zhang, F. *J. Colloid Interface Sci.* **2015**, *437*, 58−64.

(23) Ma, T. Y.; Qiao, S. Z. *ACS Catal.* **2014**, *4*, 3847−3855.

(24) Zang, D.-M.; Cao, D.-K.; Zheng, L.-M. *Inorg. Chem. Commun.* **2011**, *14*, 1920−1923.

(25) Ma, T.-Y.; Yuan, Z.-Y. *ChemSusChem* **2011**, *4*, 1407−1419.

(26) Dutta, A.; Patra, A. K.; Bhaumik, A. *Microporous Mesoporous Mater.* **2012**, *155*, 208−214.

(27) Tang, S.-F.; Pan, X.-B.; Lv, X.-X.; Yan, S.-H.; Xu, X.-R.; Lia, L.-J.; Zhao, X.-B. *CrystEngComm* **2013**, *15*, 1860−1873.

(28) Zhu, Y.-P.; Liu, Y.-L.; Ren, T.-Z.; Yuan, Z.-Y. *Nanoscale* **2014**, *6*, 6627−6636.

(29) Wharmby, M. T.; Pearce, G. M.; Mowat, J. P. S.; Griffin, J. M.; Ashbrook, S. E.; Wright, P. A.; Schilling, Lars-Hendrik; Lieb, Alexandra; Stock, Norbert; Chavan, S.; Bordiga, S.; Garcia, E.; Pirngruber, G. D.; Vreeke, M.; Gora, L. *Microporous Mesoporous Mater.* **2012**, *157*, 3−17.

(30) Fu, R.; Hu, S.; Wu, X. *CrystEngComm* **2012**, *14*, 5761−5764.

(31) Fu, R.; Hu, S.; Wu, X. *CrystEngComm* **2012**, *14*, 3478−3483.

(32) Kan, W.-Q.; Ma, J.-F.; Liu, Y.-Y.; Yang, J.; Liu, B. *CrystEngComm* **2012**, *14*, 2268−2277.

(33) Patterson, A. R.; Schmitt, W.; Evans, R. C. *J. Phys. Chem. C* **2014**, *118*, 10291−10301.

(34) Colodrero, R. M. P.; Papathanasiou, K. E.; Stavgianoudaki, N.; Olivera-Pastor, P.; Losilla, E. R.; Aranda, M. A. G.; León-Reina, L.; Sanz, J.; Sobrados, I.; Choquesillo-Lazarte, D.; García-Ruiz, J. M.; Atienzar, P.; Rey, F.; Demadis, K. D.; Cabeza, A. *Chem. Mater.* **2012**, *24*, 3780−3792.

(35) Taylor, J. M.; Mah, R. K.; Moudrakovski, I. L.; Ratcliffe, C. I.; Vaidhyanathan, R.; Shimizu, G. K. H. *J. Am. Chem. Soc.* **2010**, *132*, 14055−14057.

(36) Wegener, J.; Kaltbeitzel, A.; Graf, R.; Klapper, M.; Müllen, K. *ChemSusChem* **2014**, *7*, 1148−1154.

(37) Huang, J.; Liu, P.-Y.; Zhu, H.; Bao, S.-S.; Zheng, L.-M.; Ma, J. *ChemPlusChem* **2012**, *77*, 1087−1095.

(38) Yang, X.-J.; Bao, S.-S.; Ren, M.; Hoshino, N.; Akutagawa, T.; Zheng, L.-M. *Chem. Commun.* **2014**, *50*, 3979−3981.

(39) Zangana, K. H.; Pineda, E. M.; Vitorica-Yrezabal, I. J.; McInnes, E. J. L.; Winpenny, R. E. P. *Dalton Trans.* **2014**, *43*, 13242−13249.

(40) Zhou, T.-H.; He, Z.-Z.; Xu, X.; Qian, X.-Y.; Mao, J.-G. *Cryst. Growth Des.* **2013**, *13*, 838−843.

(41) Galezowska, J.; Gumienna-Kontecka, E. *Coord. Chem. Rev.* **2012**, *256*, 105−124.

(42) Li, C.; Jiao, C.-Q.; Sun, Z.-G.; Chen, K.; Wang, C.-L.; Zhu, Y.-Y.; Zhu, J.; Zhao, Y.; Zheng, M.-J.; Sun, S.-H.; Chu, W.; Tian, H. *CrystEngComm* **2012**, *14*, 5479−5486.

(43) Dong, D. P.; Sun, Z. G.; Tong, F.; Zhu, Y. Y.; Chen, K.; Jiao, C. Q.; Wang, C. L.; Li, C.; Wang, W. N. *CrystEngComm* **2011**, *13*, 3317−3320.

(44) Duan, K.; Fan, Y.; Wang, R. *J. Biomed. Mater. Res., Part B* **2005**, *72B*, 43−51.

(45) Liu, D.; Kramer, S. A.; Huxford-Phillips, R. C.; Wang, S.; Della Rocca, J.; Lin, W. *Chem. Commun.* **2012**, *48*, 2668−2670.

(46) Uchtman, V. A. *J. Phys. Chem.* **1972**, *76*, 1304−1310.

(47) Stavgianoudaki, N.; Papathanasiou, K. E.; Colodrero, R. M. P.; Choquesillo-Lazarte, D.; Garcia-Ruiz, J. M.; Cabeza, A.; Aranda, M. A. G.; Demadis, K. D. *CrystEngComm* **2012**, *14*, 5385.

(48) Seifullina, I. I.; Martsinko, E. E.; Aleksandrov, G. G.; Sergienko, V. S. *Russ. J. Inorg. Chem.* **2004**, *49*, 928−932.

(49) Niekiel, F.; Stock, N. *Cryst. Growth Des.* **2014**, *14*, 599−606.

(50) Rochdaoui, R.; Silvestre, J.-P.; Dao, N. Q.; Lee, M.-R.; Neuman, A. *Acta Crystallogr., Sect. C: Cryst. Struct. Commun.* **1992**, *48*, 2132−2135.

(51) Wu, Z.; Liu, Z.; Tian, P.; Yang, Y.; Xu, L.; Song, H.; Bao, X.; Liu, X.; Liu, X. *J. Cryst. Growth* **2004**, *264*, 400−408.

(52) Zheng, L.-M.; Song, H.-H.; Duan, C.-Y.; Xin, X.-Q. *Inorg. Chem.* **1999**, *38*, 5061−5066.

(53) Yi, X.-Y.; Liu, B.; Jimenez-Aparicio, R.; Urbanos, F. A.; Gao, S.; Xu, W.; Chen, J.-S.; Song, Y.; Zheng, L.-M. *Inorg. Chem.* **2005**, *44*, 4309−4314.

(54) Zhang, L.; Sun, J.; Zhou, Y.; ul Hassan, S.; Wang, E.; Shi, Z. *CrystEngComm* **2012**, *14*, 4826−4833.

(55) Yin, P.; Gao, S.; Zheng, L.-M.; Wang, Z.; Xin, X.-Q. *Chem. Commun.* **2003**, 1076−1077.

(56) Yi, X.-Y.; Zheng, L.-M.; Xu, W.; Feng, S. *Inorg. Chem.* **2003**, *42*, 2827−2829.

(57) Rocha, J.; Paz, F. A. A.; Shi, F.-N.; Ferreira, R. A. S.; Trindade, T.; Carlos, L. D. *Eur. J. Inorg. Chem.* **2009**, 4931−4945.

(58) Tan, H.; Chen, W.; Liu, D.; Li, Y.; Wang, E. *Dalton Trans.* **2010**, *39*, 1245−1249.

(59) Yang, W.; Wu, H.-Y.; Wang, R.-X.; Pan, Q.-J.; Sun, Z.-M.; Zhang, H. *Inorg. Chem.* **2012**, *51*, 11458−11465.

DOI: 10.1021/ic5029993
Inorg. Chem. 2015, 54, 4268−4278

(60) Liu, B.; Li, B.-L.; Li, Y.-Z.; Chen, Y.; Bao, S.-S.; Zheng, L.-M. *Inorg. Chem.* **2007**, *46*, 8524−8532.
(61) Bruker AXS. *APEX2, V2008.6; SADABS V2008/1; SAINT+ V7.60A; SHELXTL V6.14;* Bruker AXS Inc.: Madison, WI, 2008.
(62) Cheng, P.-C.; Lin, W.-C.; Tseng, F.-S.; Kao, C.-C.; Chang, T.-G.; Senthil Raja, D.; Liu, W.-R.; Lin, C.-H. *Dalton Trans.* **2013**, *42*, 2765−2772.
(63) Zima, V.; Senthil Raja, D.; Lee, Y.-S.; Chang, T.-G.; Wu, C.-Y.; Hu, C.-C.; Lee, K.-R.; Lai, J.-Y.; Yeh, J.-M.; Lin, C.-H. *Dalton Trans.* **2013**, *42*, 15332−15342.
(64) Spek, A. L. *J. Appl. Crystallogr.* **2003**, *36*, 7−13.
(65) *Joint Committee on Powder Diffraction Standards;* International Centre of Diffraction Data: Swarthmore, PA. Online: http://www.icdd.com/profile/overview.htm.
(66) Cotton, S. *Lanthanide and Actinide Chemistry;* Wiley: Chichester, U.K., 2006.
(67) Wang, C. M.; Lii, K. H. *Inorg. Chem.* **2009**, *48*, 6335−6337.
(68) Tang, S. F.; Song, J. L.; Li, X. L.; Mao, J. G. *Cryst. Growth Des.* **2006**, *6*, 2322−2326.

DOI: 10.1021/ic5029993
Inorg. Chem. 2015, 54, 4268−4278